CHAPTER 7: INTERCOMPARISON OF NUMERICAL MODELS OF FLARING CORONAL LOOPS

R.A. Kopp, G.H. Fisher, P. MacNeice, R.W.P. McWhirter, and G. Peres

7.1 INTRODUCTION

The past decade of solar observations from space, which has seen the extension of high spatial resolution and temporal cadence into the XUV spectral regime, has demonstrated convincingly that the corona is pervaded at all times by loop-shaped features that appear to be closely aligned with ambient magnetic field lines. This structuring is most strikingly evident in solar active regions. Together with photospheric magnetograms, the orientations of these loop structures allow the magnetic topology of much of the corona to be mapped out in detail. Whereas some fraction of the coronal volume may be permeated by open field lines or may even be virtually field-free, the plasma contained therein is of a lower density than that contained on the loops and is thereby more difficult to diagnose. Consequently, most interpretative studies have concentrated on the development and application of loop models to active region phenomena. Especially important to devise, but nonetheless difficult, are quantitative models for describing temporal changes of the plasma resulting from, for example, fluctuations of loop energy input. The extreme case is that which occurs during a solar flare, when the energy supply of a given magnetic loop may vary by many orders of magnitude on a time scale of a few seconds or less.

At the first meeting of the SMM Flare Workshop (23-28 January, 1983) it became apparent that, among the many efforts currently underway around the world to simulate various flare-related phenomena using large computer codes, several groups seemed to be in a fairly advanced state in their capabilities to carry out calculations relevant to the problem mentioned above—namely, the hydrodynamic and radiative response of a single magnetic flux tube to a sudden release of energy within it. This led rather quickly to the idea of using the SMM Flare Workshop Series as a forum for the intercomparison of code calculations on a specific standardized loop-heating problem. Such an opportunity, whereby a large group of numerical analysts from the international solar physics community gathers simultaneously, seldom presents itself in the everyday course of events. Even on the rare occasion when it does, the atmosphere is usually not conducive to an honest self-appraisal of code capabilities and, perhaps more importantly, of inherent limitations. The work to be summarized here represents the principal activity of the Flare Dynamical Modeling Group (FDMG) of the SMM Workshop—the seventh group organized for the purpose of studying various aspects of the flare process. This Modeling Group, however, was unique in that its members were drawn from each of the other six groups. Whereas this posed severe constraints on the amount of time available for the required discussions, it carried the advantage of representing the expertise of all segments of the Workshop at large.

7.2 THE ORIGINAL BENCHMARK PROBLEM

The physical configuration which the FDMG participants agreed to consider was chosen to be simple enough that all of the applicable computer codes could be used with only minor modifications, yet sufficiently complex that the basic nonlinear processes believed to govern the physics of real loops (radiation, thermal conduction, compressible hydrodynamics, gravity, nonthermal heating) could be incorporated with some degree of realism. However, it should be kept in mind that the so-called "Benchmark Model" which resulted is nothing more than an attempt to establish a baseline calculation against which the performance of a given code might be judged. It was hoped thereby to provide a means for quantitatively comparing one code calculation with another. The model, on the other hand, was specifically *not* meant to represent either an average or a particular flare loop observed by the SMM or by anyone else, although of course to keep the problem interesting the choice of physical parameters was dictated by the conditions believed to typify flare loops in general.

The proposed Benchmark Problem consists of an infinitesimal magnetic flux tube containing a low-beta plasma. The field strength is assumed to be so large that the plasma can move only along the flux tube, whose shape remains invariant with time (i.e., the fluid motion is essentially one-dimensional). The flux tube cross section is taken to be constant over its entire length. In planar view the flux tube has a semi-circular shape, symmetric about its midpoint $s = s_{max}$ and intersecting the chromosphere-corona interface (CCI) perpendicularly at each footpoint; see Figure 7.2.1a. The arc length from the loop apex to the CCI is 10,000 km. The flux tube extends an additional 2000 km below the CCI to include the chromosphere, which initially has a uniform temperature of 8000 K. The temperature at the top of the loop was fixed initially at 2×10^6 K. The plasma is assumed to be a perfect gas ($\gamma = 5/3$), consisting of pure hydrogen which is considered to be fully ionized at all temperatures. For simplicity, moreover, the electron and ion temperatures are taken to be everywhere equal at all times (corresponding to an artificially enhanced electron-ion collisional coupling).

The equations describing the one-dimensional temporal evolution of the loop plasma are:

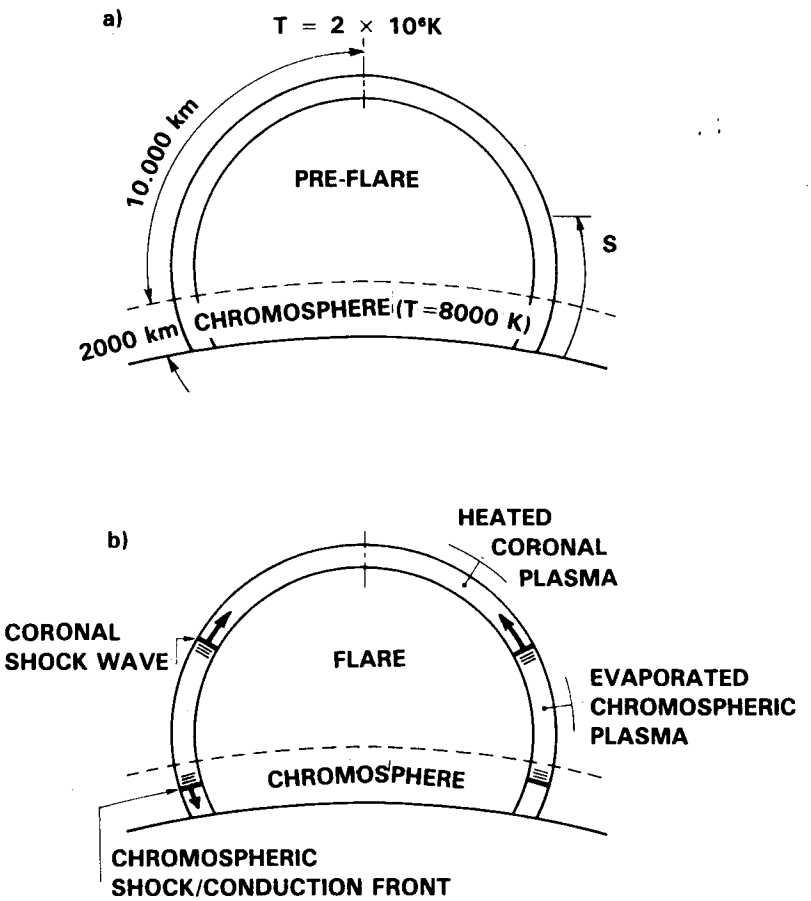

Figure 7.2.1 Schematic plan view of the loop configuration used in the Benchmark Problem (a) before and (b) after the initiation of the flare energy release.

$$\frac{\partial \varrho}{\partial t} + \frac{\partial}{\partial s}(\varrho v) = 0 \qquad (1)$$

$$\varrho \frac{Dv}{Dt} = -\frac{\partial P}{\partial s} - \varrho g_{\parallel} \qquad (2)$$

$$\frac{3}{2}\frac{DP}{Dt} = H(s,t) - N_e^2 \Lambda(T) + \frac{\partial}{\partial s}\{K(T)\frac{\partial T}{\partial s}\} - \frac{5}{2}P\frac{\partial v}{\partial s}, \qquad (3)$$

where N_e is the electron density, $P = 2N_e kT$ is the gas pressure, $\varrho = m_p N_e$ is the plasma density, and v is the fluid velocity; $g_{\parallel}$ is the component of gravity tangential to the loop. Moreover, s denotes arc length from the loop footpoint and D/Dt represents the time derivative following a fluid element as it moves. H(s,t) denotes the nonthermal heating per unit volume (see below), $N_e^2 \Lambda(T)$ is the (optically thin) radiative loss function, and K(T) is the plasma thermal conductivity.

For the radiative losses, $\Lambda(T)$ was chosen to approximate the form for a plasma with normal solar abundances, viz.,

$$\Lambda(T) = 3\times10^{-22}\,(T/(2\times10^4))^3 \;\ldots\ldots\; (T \le 2\times10^4\ \mathrm{K}) \qquad (4a)$$

$$\Lambda(T) = 3\times 10^{-22} \;\ldots\ldots\; (2\times10^4 \le T \le 2\times10^5\ \mathrm{K}) \qquad (4b)$$

$$\Lambda(T) = 3\times10^{-22}\,(T/(2\times10^5))^{-1/2} + 2\times10^{-23}\,(T/10^8)^{1/2} \cdots\cdots\; (T \ge 2\times10^5\ \mathrm{K}). \qquad (4c)$$

The initially steady preflare state of the loop is maintained by a nonthermal heating function $H_o(s)$ with the following properties:

i. in the chromosphere, that necessary to balance radiative losses at each point, thereby maintaining isothermal conditions;

ii. above the chromosphere, a constant value such that the net energy input exactly balances the integrated radiative losses from the corona and transition region.

The thermal conductivity was taken to be of the classical Spitzer form—$K(T) = 9.203 \times 10^{-7}\, T^{5/2}$—and the resulting heat flow was assumed not to be flux-limited.

Along with the various solar constants (gravity, radius, etc.), the above details prescribe the quiescent thermodynamical state of the loop plasma that persists up to, say, t = 0. To initiate a transient response an additional input of energy was invoked at later times; the net heating function was taken to be of the form

$$H(s,t) = H_0(s) + H_F(s,t), \qquad (5)$$

where

$$H_F(s,t) = \begin{cases} E \exp[-(s-s_{max})^2/\sigma^2] & (0 \le t \le 5\ s) \\ 0. & (t \ge 5\ s) \end{cases} \qquad (6)$$

The gaussian width of deposition, σ, was chosen to have the value 5000 km, and the constant E was to be determined by the condition that the integral of H_F over either half of the flux tube correspond to a transient energy flux of 10^{11} erg cm^{-2} s^{-1}, a not flare-unlike value.

The anticipated dynamical response of the loop atmosphere to this transient heating function is depicted by the general scenario of Figure 7.2.1b and can be described qualitatively as follows. For the assumed value of σ, nearly all of the flare energy is deposited in the corona. This leads to a rapid rise in the coronal temperature from its initial value on a time scale given by $\tau_F = 3N_e kT/E \simeq 0.02$ s, which is much less than the acoustic transit time for the loop: $\tau_a\, s_{max}/c \simeq 50$ s. Thus, much of the heating takes place before substantial mass motions can occur. The temperature rise is most rapid near the loop top (where the heating is strongest), and this drives a supersonic thermal wave downward along the loop (cf. Figure 7.2.2). When this conduction front reaches the top of the chromosphere, the resultant sudden heating of the cool plasma there causes an expansion in both directions along the flux tube. The downward-propagating pressure wave rapidly steepens to form a shock, which ultimately overtakes the thermal wave as both move deeper into the chromosphere. At the same time, the upward-moving (evaporated) chromospheric plasma pushes a weaker pressure wave ahead of it into the corona. This wave may or may not have time to steepen into a shock before reaching the top of the loop. In any case, the loop soon becomes filled with hot and dense matter. It was agreed by all participants to try to follow the dynamical history of the loop plasma for a period of ten seconds following the switch-on of the transient heating function.

7.3 INITIAL SOLUTION COMPARISONS

Originally eight groups or individuals expressed confidence in their ability to perform the above calculation in advance of the second SMM Workshop (9-14 June 1983). These are listed alphabetically by name of the principal worker in Table 7.3.1. By the time of this second gathering

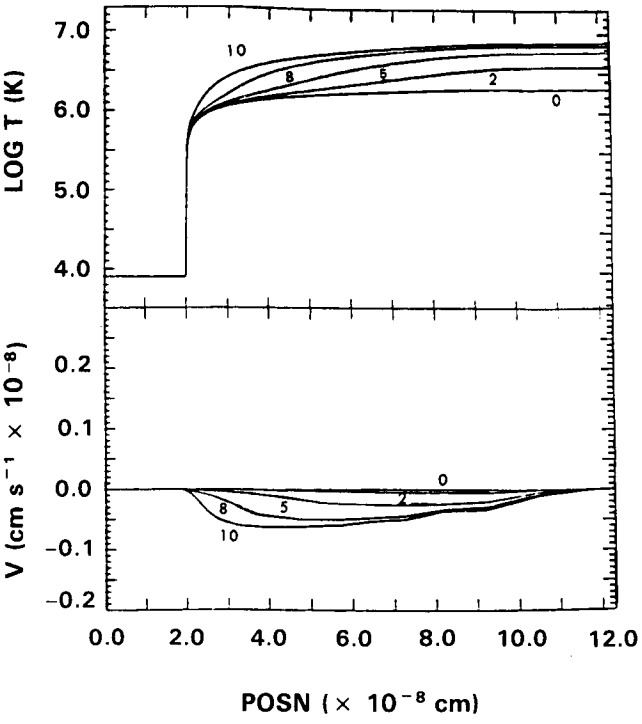

Figure 7.2.2 Loop temperature and velocity profiles at various times during the first 10 s of the transient flare heating, as calculated by P. MacNeice (CAMB) for the final Benchmark Problem parameters. The density profile changes but little from that of the initial state during this time and thus is not shown here.

an initial comparison of the solution curves had been assembled at Rutherford Laboratory, from which it became immediately apparent that large discrepancies existed among the various calculations. In fact, while there was more-or-less unanimous agreement as to certain global properties of the system behavior (peak temperature reached, thermal-wave time scales, etc.), no two groups could claim satisfactory accord when a more detailed comparison of solutions was attempted.

As a result of discussions held during the second Workshop, it was concluded that some of the differences between solutions could be accounted for by the realization that, even though purportedly agreed to in advance, no two groups had actually solved exactly the same problem. For example, MSFC had used a thermal conduction flux limiter; PLRMO had inadvertently spread the transient heat input over too much of the loop; and LANL, GSFC, and NRL had secretly "modified" the radiative loss function at low temperatures (albeit in different ways) from that given above, to stabilize the initial atmosphere against an apparent tendency to heat up almost explosively (a behavior explained subsequently by PLRMO and UCSD as being caused by an unrealistic prescription of the quiescent heating function; see below). However, not all of the discrepancies could be accounted

Table 7.3.1 Benchmark Calculation Participants

Name	Institute	Identifier	Type of Code
C.C. Cheng	Naval Research Laboratory	NRL	Eulerian (FCT)
G.H. Fisher	Univ. of Calif., San Diego	UCSD	Lagrangian
R.A. Kopp	Los Alamos National Laboratory	LANL	Lagrangian
P. MacNeice	Cambridge University	CAMB	Eulerian (FCT)
F. Nagai	Marshall Space Flight Center	MSFC	Eulerian
G. Peres	Osserv. Astronomico, Palermo	PLRMO	Eulerian
A.I. Poland	NASA-Goddard Space Flight Center	GSFC	Eulerian (FCT)
D.F. Smith	Berkeley Research Associates	BRA	Eulerian

for by these differences. It was generally felt by the FDMG participants that none of the numerical solutions which had been carried to completion were to be wholly trusted, because each had failed to resolve adequately the structure of the thermal wave front once it enters the chromosphere; as was pointed out by Fisher (UCSD), for the adopted flare heat input one would expect this front to have a thickness of only about 10 cm! Even were it possible to resolve the front region, say by means of an automatic dynamic rezoner (only the UCSD code had this capability), the small time steps which would be required to achieve reasonable solution accuracy would have rendered the calculation impractical on present-day computers.

The issue of numerical resolution of the thermal wave front is a complex one. If it could be demonstrated that the structure of this front is not important to the global dynamics of the loop plasma, then one might be able to introduce a numerical thermal conductivity to spread out the front artificially over a few mesh points, analogous to the use of an artificial viscosity for shockwave problems. On the other hand, if the detailed structure of the thermal front turns out to be important for determining the global behavior (e.g., the net evaporation rate or the peak coronal temperature), then it is essential to resolve the front even if one is interested *only* in the global properties of the loop. Studies by McClymont and Fisher (UCSD) indicate that, if the total energy flux into the corona is large compared with coronal radiative losses, then it is not essential to resolve the thermal front to get the correct evaporation rate and coronal temperature. However, once sufficient evaporation has taken place that the total coronal radiative loss rate is of the same magnitude as the total coronal energy flux, the subsequent numerical solution of the evaporation problem is grossly incorrect unless the thermal front *is* resolved.

But these considerations aside, it was recognized that the posed problem is also physically unrealistic for various reasons. For example, linear heat flow theory (as exemplified by the use of the Spitzer conductivity) does not even apply in regions of strong thermal gradients; instead, the actual heat flow will be flux-limited and, ideally, a description of heat flow based on "non-local" properties of the atmosphere should be used. Lacking such, one can rightfully question the significance of numerical heat-flow simulations for which the mesh size required for numerical accuracy/stability is much smaller than an electron mean free path. However, the primary goal of the Benchmark Model was to intercompare code calculations on a standardized, although hypothetical, problem, rather than to establish the best possible physical model. To this end, it was decided to repeat the basic Benchmark Model calculation for the third and final Workshop meeting (13-17 February, 1984), using a transient energy flux reduced by two orders of magnitude from the original value. This would have the effect of driving a much gentler thermal wave into the chromosphere; since the thickness of the wave front increases with decreasing thermal energy flux, adequate numerical resolution of this front was now expected to pose less of a constraint on obtaining a solution. It was moreover agreed to leave the transient heating on for the duration of the problem, which was extended to 100 s from the original 10 s (thus, the total "flare" input was smaller than that of the original problem by only a factor of 5). Although the thermal wave front in the problem as redefined is still quite thin, it was nevertheless felt that the codes with dynamic rezoners might at least have a chance of running to completion with the finite computer resources available.

Interestingly, whereas the intercomparison of this second round of calculations showed a modest improvement in agreement, the improvement was not as marked as expected. Still there were found to be large differences in the velocity of the evaporated chromospheric plasma, and even the temperature at the top of the loop—perhaps the least sensitive parameter used in the comparison—varied considerably from one solution to the next. Herein was realized a second major problem—this one associated with the basic definition of the quiescent heating function for the pre-flare atmosphere. Recall that this was chosen arbitrarily to be a time-independent "volumetric" heating function (i.e., the units are erg cm^{-3} s^{-1}) of position s along the flux tube, and that it was to be left on at all times. A plot of this function against height shows a steep exponential decrease up through the chromosphere—a direct result of the small density scale height there—followed by a discontinuous drop by an order

of magnitude to its (assumed) uniform coronal value for $s \geq 2000$ km. It is this sudden jump that plays havoc with numerical codes. For, even without a transient heat input, finite-difference errors will cause the pre-flare atmosphere to be slightly out of hydrostatic equilibrium (by a varying degree with each code) and some initial readjustment of the density structure will inevitably occur. Consider, for example, the result of such an adjustment by which the corona settles downward ever so slightly, compressing the chromosphere below. The coronal plasma which was originally just above 2000 km now finds itself in the region of strong chromospheric heating, but being of much lower density than the chromosphere is incapable of radiating away this increased heat input. Consequently, the temperature of this region begins to rise; the resulting localized pressure enhancement initiates an outward expansion of the plasma, causing the density to decrease still further and the heating to become even more unbalanced. This unstable situation rapidly leads to expansion of an almost explosive nature.

The same argument can be used to show that, were finite-difference errors nonexistent and the pre-flare atmosphere perfectly in equilibrium, the initiation of transient heating would still cause an unrealistically violent expansion of the upper chromosphere to take place immediately upon arrival of the leading edge of the thermal wave in these layers. As was originally suggested by George Fisher (UCSD), this unphysical behavior can be largely avoided by using a quiescent heating function which is defined (and kept constant) per unit mass rather than per unit volume. Then, when the plasma starts to expand as the result of a heating imbalance, the amount of (quiescent) heating of each mass element will remain constant and radiative losses will be better able to restrict a further temperature rise.

The extreme sensitivity of the plasma behavior to the adopted definition of the quiescent heating function was illustrated most vividly via a calculation carried out by Giovanni Peres (PLRMO). Therein the original volumetric heating function was divided by the mass density at each point to give an equivalent heating function per unit mass, and the dependence of this function on position was kept constant throughout the calculation (the simplest procedure when using an Eulerian code). In the original (volumetric heating) case the temperature at the top of the loop continued to increase at late times as chromospheric evaporation, supplied ever-faster by the quiescent heating function, grew rapidly in intensity, whereas with the revised definition the temperature approached a well-defined limit. Other properties of the solution changed by even greater amounts. Thus a seemingly minor change of definition of the quiescent heating function was shown to have a dramatic effect on the temporal evolution of the loop plasma.

Why didn't the other groups experience the same difficulties with "explosive" evaporation as did PLRMO? Confronted with the above results, it turned out that nearly all had. For example, UCSD, being probably the first to identify the problem but unable to convince others of its importance, had decided early on to abandon the volumetric heating function in favor of one defined per unit mass. And, as mentioned earlier, several groups had independently chosen to "modify" their radiative loss function so that it vanished at chromospheric temperatures; since the magnitude of the chromospheric heating function is determined by the condition that it balance radiative losses at each point, this procedure clearly eliminates the problem, although in an artificial manner.

7.4 FINAL BENCHMARK PROBLEM AND SOLUTION COMPARISON

With these facts in hand, it was decided at the final Workshop that those participants who hadn't already done so, and who were willing and able, would perform a final calculation using a quiescent heating function properly defined per unit mass. Even so, one realized by now that certain intrinsic differences between Lagrangian and Eulerian code logistics would make impractical a precise comparison of results; a quiescent heating function that "remains constant in time" is interpreted differently by the two approaches. Nevertheless, it was expected that even a rough comparison of results would yield substantially closer agreement than had been obtained previously.

This expectation was in fact borne out. Figures 7.4.1–7.4.4 show some of the results of the final comparison, completed some time after the end of the third Work-

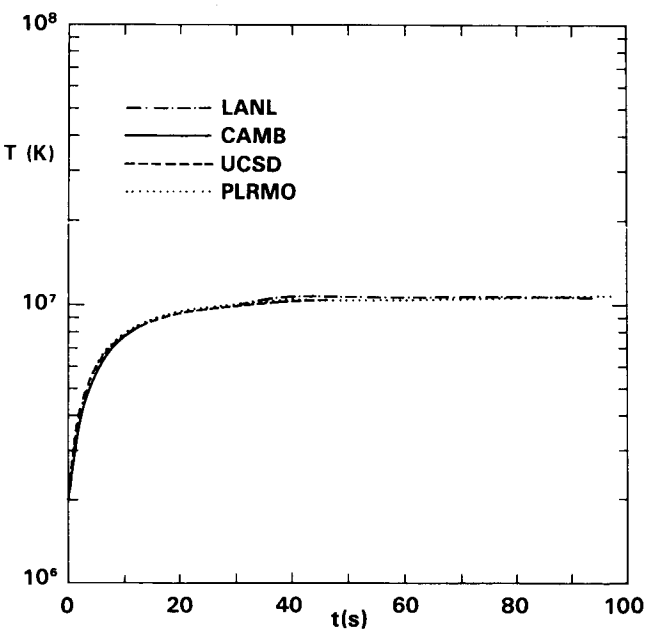

Figure 7.4.1 Temperature versus time at the top of the loop, as predicted by the four codes used for the final Benchmark Model calculation.

shop. We note first that the number of participants has diminished markedly, from the original eight to now only four. The quantities displayed are arranged roughly in order of increasing discrepancies between solutions. For example, all calculations are now in close accord as to the time history of temperature at the loop top; this quantity is primarily a function of the total loop heat input. On the other hand, appreciable differences are seen to persist in the maximum electron density reached in the chromospheric shock wave, a result which is not too surprising in view of the fact that this quantity is quite sensitive to the particular grid spacing used to resolve the shock wave (which varied considerably from one calculation to another).

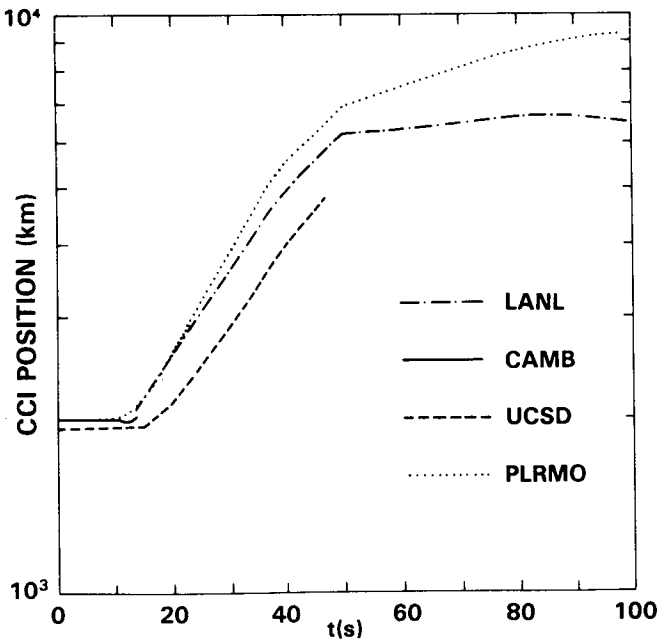

Figure 7.4.2. Height of the original chromosphere-corona interface (CCI) as a function of time.

Thus, the results shown in Figures 7.4.1–7.4.4 comprise in fact a "Benchmark Model" against which other flare-loop codes can be tested for the loop heating problem described here. The specific parameters used for this problem are collected in Table 7.4.1.

Nevertheless, it is important to note that significant discrepancies remain between the code results, as shown in Figures 7.4.2–7.4.4. Whereas this is not particularly comforting to those individuals who performed the calculations, it is important that these results be presented in the form shown here rather than for example, as an "averaged" solution, because the adopted format conveys some notion of the inherent uncertainties that still exist in the Benchmark Model. Future numerical solutions of the Benchmark Problem, either by the original participants or by others, should be aimed at resolving these remaining discrepancies.

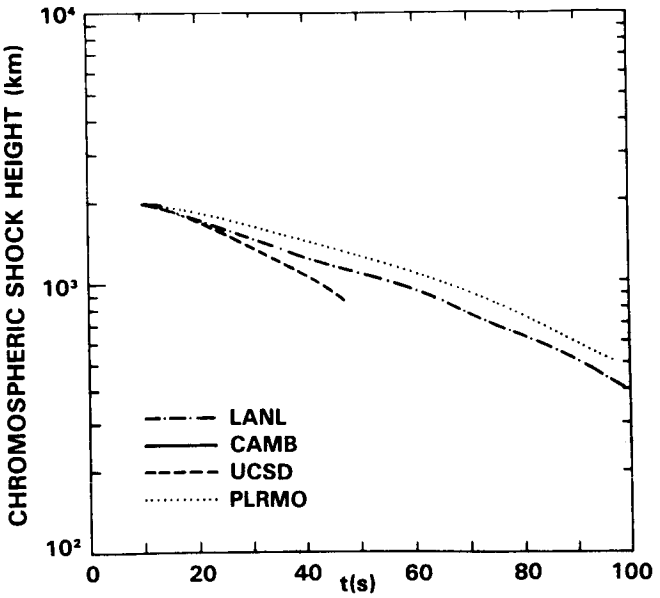

Figure 7.4.3 Position of the downward-propagating shock wave in the chromosphere. Note that this shock first appears at about 10 s in all the calculations, i.e., when the thermal wave first reaches the top of the chromosphere.

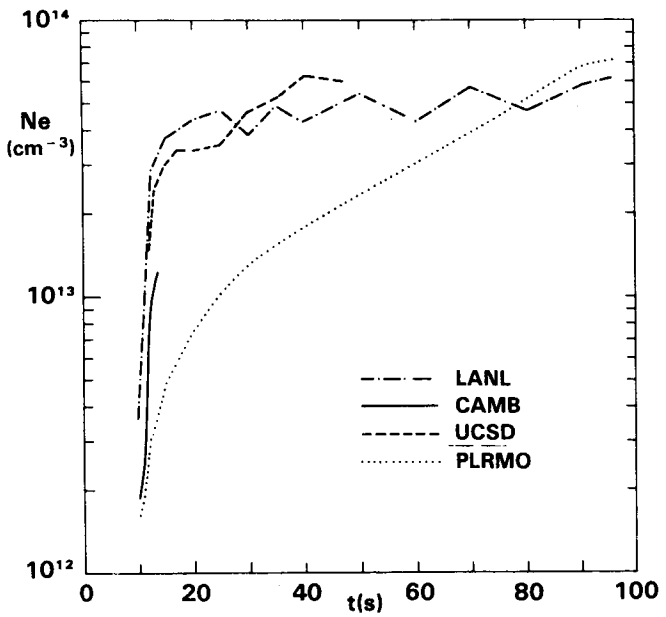

Figure 7.4.4 Maximum electron density reached behind (i.e., just above) the chromospheric shock front.

7.5 CONCLUSIONS

The flare modeling activity at the SMM Flare Workshop Series represented the dedicated efforts of several individuals and substantial computer resources of their respective institutions. Whereas these have not yet converged upon a

Table 7.4.1 Benchmark Problem — Definition and Parameters

1. Symmetric semi-circular loop of uniform cross section—cf. Figure 7.2.1a

   s_{max} = 2000 km (chromosphere) + 10,000 km (corona).

2. Fully ionized hydrogen atmosphere (perfect gas)—$N_i = N_e$; $T_i = T_e$.

3. Optically thin radiative losses—cf. Equations (4a-c).

4. Spitzer thermal conductivity (no flux limit imposed)

   $K(T) = 9.203 \times 10^{-7}\ T^{5/2}$ erg cm^{-1} s^{-1} K^{-1}.

5. Initial atmosphere

   a. Hydrostatic equilibrium ($g = 2.738 \times 10^4$ cm s^{-2}):

   $$\frac{\partial}{\partial t} = 0;\ v = 0;\ \frac{dP}{ds} = -\varrho g_{\parallel}.$$

   b. Isothermal chromosphere ($0 \leq s \leq 2000$ km):

   $T = 8000$ K; $H_o(s) = N_e^2\ \Lambda(T)$.

   c. Corona (2000 km $\leq s \leq s_{max}$):

   $T = 8000$ K at chromospheric boundary ($s = 2000$ km);

   $T = 2 \times 10^6$ K and $\frac{dT}{ds} = 0$ at loop top ($s = s_{max}$);

   $H_o(s)$ = a constant such that $H_o \int ds = \int N_e^2\ \Lambda(T)\ ds$, where the integrals extend over $(2000, s_{max})$.

6. Flare heating function

   $H_F(s,t) = H_F(s) = E \exp[-(s-s_{max})^2/\sigma^2]$, where $\sigma = 5000$ km and $E = 2 \times 10^9/(\sigma\sqrt{\pi})$ erg cm^{-3} s^{-1};

   Flare heating left on for 100 s, the problem run time.

unique Benchmark Model, we *have* succeeded in defining a well posed Benchmark Problem, and this is a necessary first step. Future modeling work directed toward this problem will no doubt produce the desired unique solution. Perhaps more valuable than this was the general recognition within the flare-modeling community of certain pitfalls and difficulties associated with trying to model the energetic flare process numerically. In particular, we call attention once more to the importance in any calculation of confronting directly the difficult numerical problems associated with the rapid motion of a very steep thermal wave front through the chromosphere, as well as that of the extremely thin, dense compression wave that runs ahead of it.

In addition, we have learned how difficult it is to intercompare the results obtained with diverse and highly complex computer codes. This is partly due to the intrinsic differences in mathematical formulation used by various codes (Eulerian versus Lagrangian hydrodynamics, fixed-nonuniform zoning versus adaptive rezoning, etc.), which render a detailed comparison of many quantities impossible without making fairly major code modifications or extensions. But this is not an insoluble dilemma. Perhaps the most important lesson learned is how careful one must be to define a meaningful problem in the first place, the solution of which will provide a viable test of real simulational capabilities and not just magnify seemingly insignificant differences of problem definition to the point where these dominate the results.

Finally, it was felt by all participants that, although an attempt had been made to reduce the Benchmark Problem to its bare essentials, it would nevertheless be useful to have

available a selection of even simpler test problems, for the purpose of verifying the mechanics of a given code for each elementary physical process by itself. The following list is by no means all inclusive. We simply reference here a few situations for which analytical solutions (e.g., similarity solutions) are known, without elaborating on any of them. Of course, the value of these solutions is limited to codes which (a) possess the capability of switching off all physical processes except that which is being checked, and (b) can accommodate the required boundary conditions.

1. Thermal-wavefront dynamics (no hydrodynamics or radiation). In a medium with nonlinear heat conduction, the presence of transient energy sources can give rise to steep thermal fronts (Marshak waves) which propagate away from the source regions and transport energy to other parts of the problem. Useful similarity solutions can be found in References 1 and 2.
2. Continuum hydrodynamics (i.e, no shock waves) with gravity. For the case of one-dimensional time-dependent flow with a prescribed (fixed) temperature profile and flowtube geometry, a type of similarity solution has been given by Reference 3; the flow velocity at each point is time-invariant, but the density grows or decays exponentially with time.
3. Shockwave dynamics (no heat conduction or radiation). Besides the obvious requirement that the Rankine-Hugoniot conditions be satisfied across a shock front, a simple test case that addresses the interaction of a flow discontinuity with a problem boundary is that of reflection off a rigid wall of a piston-driven shock wave (Ref. 4).
4. Optically thin radiation (no fluid motions or heat conduction). The obvious test here would be to simulate numerically the analytical form of the radiative cooling curve:

$$T(t) = \{T_o^{1-n} + \frac{(n-1)A}{3k} N_e t\}^{\frac{1}{1-n}},$$

which results from solving the energy equation for the case that $\Lambda(T) = A T^n$, where A and n ($\neq 1$) are prescribed constants.

7.6 REFERENCES

1. Richtmeyer, R. D. and Morton, K. W.: 1967, *Difference Methods for Initial Value Problems*, Interscience, New York, pp. 201-206.
2. Zel'dovich, Ya. B. and Raizer, Yu. P.: 1967, *Physics of Shock Waves and High-Temperature Hydrodynamic Phenomena*, Vol. II, Academic Press, New York, pp. 652-684.
3. Kopp R. A.: 1980, Solar Phys. *68*, 307.
4. Landau, L. D. and Lifshitz, E. M.: 1959, *Fluid Mechanics*, Pergamon Press, London, p. 365.